Open Access Library Journal
2017, Volume 4, e3909
ISSN Online: 2333-9721
ISSN Print: 2333-9705

Structural and Optical Properties Evolution of Au/SiO_2 Nanocomposite Films: The Influence of Substrate Temperature and Thermal Annealing

Ahmed Belahmar[1], Ali Chouiyakh[1*], Mounir Fahoume[2]

[1]Department of Physics, Renewable Energy and Environment Laboratory, Faculty of Science, Ibn Tofail University, Kenitra, Morocco
[2]Department of Physics, Laboratory of Condensed Matter Physics, Faculty of Science, Ibn Tofail University, Kenitra, Morocco
Email: *ali_chouiyakh@hotmail.com

How to cite this paper: Belahmar, A., Chouiyakh, A. and Fahoume, M. (2017) Structural and Optical Properties Evolution of Au/SiO_2 Nanocomposite Films: The Influence of Substrate Temperature and Thermal Annealing. *Open Access Library Journal*, **4**: e3909.
https://doi.org/10.4236/oalib.1103909

Received: August 26, 2017
Accepted: September 25, 2017
Published: September 28, 2017

Abstract

Au/SiO_2 nanocomposite films, studied in this work, were prepared by RF-magnetron sputtering technique on glass substrate at room temperature under two different substrate temperatures (Ts), and subsequent heat treatment. For the deposited sample at T_S = 25˚C, no apparent surface plasmon resonance peak could be observed. After annealing, optical absorption spectrum of the Au/SiO_2 thin films showed a broad absorption band around 500 nm relating to gold nanoparticles without any modification in the position of the SPR and the size of particles. For the series deposited at T_S = 400˚C, the surface plasmon resonance (SPR) was found at 500 nm. After heat treatment it's redshift from 500 nm to 503 nm, while the size increases from 2.01 nm to 2.3 nm. We have also shown that, as the AuNPs are embedded in silica films, the small nanoparticles size have a slightly larger expansion coefficient than for bigger one.

Subject Areas

Composite Material, Material Experiment

Keywords

Gold Nanoparticles, Sputtering, Substrate and Annealing Temperature, Size, SPR

1. Introduction

Metallic nanoparticles possess unique optical, electronic, chemical, and magnetic properties that are different from those of individual atoms as well as their bulk

counterparts. Noble metal nanoparticles embedded in dielectric matrices exhibit a strong absorption band in UV-visible region [1] [2]. This band results when the incident photon frequency is resonant with the collective oscillation of the conduction band electrons and is known as the surface plasmon resonance (SPR) [3] [4]. The SPR frequency is strongly dependent upon the size, shape, interparticle interactions, dielectric properties, and local environment of the nanoparticle [5] [6] [7] [8]. To give a clear description of the surface plasmon absorption band and the main factors impacting its position, intensity and broadness, numerous works have been done. Particularly, studies of metal clusters with dimensions in the range 1 - 10 nm, help to determine the transition from typical properties of bulk metals to the properties of isolated atoms, and because all noble metal field applications, use very small metal particles.

The temperature dependence of optical properties of metal nanoparticles is a precondition for the development of successful and reliable applications and devices. The temperature effects on SPR absorption band in metal nanoparticles were studied e.g. by Kreibig [9], Doremus [10] [11], and the origin of temperature effects upon the SPR was analyzed by Mulvaney [12]. Link and El-Sayed also studied the temperature dependence of the SPR energy and bandwidth for gold colloidal nanoparticles within the size range of 9 nm up to 99 nm [13]. No significant influence of the temperature on the SPR energy and bandwidth was found. Nanocomposite films consisting of metal particles such as gold embedded in a silica matrix have recently been the subject of many studies [14]-[29]. A large number of methods have been used to obtain AuNPs embedded in SiO_2 films, such ion implantation [14] [15], sol-gel [16], plasma enhanced chemical vapor deposition (PECVD) [17], hybrid techniques combining pulsed-DC sputtering and PECVD, which is used for simultaneous Au sputtering and SiO_2 deposition [18] [19], and RF magnetron sputtering [20]-[29]. The flexibility and easy fabrication of diverse composite films are the advantages of sputtering method. The important factors to influence the formation of AuNPs are the distance between the target and the substrate, rf-power, sputtering time, the substrate temperature, applied voltage, and working pressure.

In our recent work [30], we have studied the temperature dependence of SPR in the gold nanoparticles in the alumina matrix. We observed the noticeable red shift of the SPR and size of Au nanoparticles with increasing temperature.

In this paper, we investigate the influence of substrate temperature and thermal annealing on the structural and optical properties of gold/silica composite films grown by RF-magnetron sputtering technique.

2. Experimental Methods

The samples, consisting of gold/silica composite thin films, were prepared by conventional radio-frequency magnetron sputtering method using an Alcatel SCM 650 apparatus. The target consisted of pure (99.99%) metal Au chips on top of a 50 mm diameter silica disc placed 60 mm away from the substrates.

Table 1. Films growth conditions.

Working argon pressure (mbar)	2×10^{-3}
Initial pressure(mbar)	1×10^{-6}
Au target (%)	2.6
Bias (V)	−50
Power (W)	50
Substrate Temperature	25˚C and 400˚C
Annealing Temperatures	300˚C - 500˚C

Sputter deposition, in a radio frequency (13.56 MHz) machine, has been carried out after the chamber reached a base pressure of (1×10^{-6}) mbar. Deposition was carried out at fixed argon pressure 2×10^{-3} mbar and at two different substrate temperatures 25˚C and 400˚C. The relevant growth conditions of the films are shown in Table 1. Under these conditions, two sets of samples are prepared and they are denoted A_1 (Ts = 25˚C) and A_2 (Ts = 400˚C). The as-deposited composite films were annealed at different temperatures of 300˚C, 400˚C and 500˚C in atmospheric pressure for 1 h.

Crystalline phase of films were determined by X-ray diffractometry (XRD), using a Siemens D5000 diffractometer, with CuKα radiation (λ = 0.15406 nm) and a Bragg-Brentano geometry. The diffraction patterns were collected over the range $10^\circ < \theta < 80^\circ$ at room temperature. The identification of Au crystalline phases was done using the JCPDS database cards $(n\_04-0784)$. Optical absorption measurements of the prepared samples were registered by a Shimadzu UV30101PC spectrophotometer, in near ultra-violet-visible-near infrared (NIV-VIS-NIR) in a range of 200 - 2000 nm wavelength.

3. Results and Discussion

3.1. Structural Characterization

Figure 1 shows the XRD patterns of the samples deposited at two substrate temperatures 25˚C and 400˚C. X-ray diffractogram of gold thin film with a cubic structure, presented as a reference, is also reported in Figure 1. From the diffractograms of all the samples, it is evident that there are no Bragg reflections that are clearly visible in the spectra but a shoulder in the range 35˚ - 47˚ and a broad peak at $2\theta = 64^\circ$ were observed, due to the small AuNPs.

From Figure 1, it is difficult to determine crystalline phases and size. However, using a commercial software program available on our computer, the XRD patterns were deconvoluted, assuming pseudo-Voigt functions in order to obtain the peak position intensity and full width at half maximum (FWHM). Note that the purpose of the deconvolution is to fit the measured XRD spectrum in well-defined peaks to which a physical meaning can be attributed. For more details see the works [22]. Figure 2 shows the curve fitting of the XRD spectrum of A_2 series. Outside the peak assigned to amorphous silica film, the diffraction

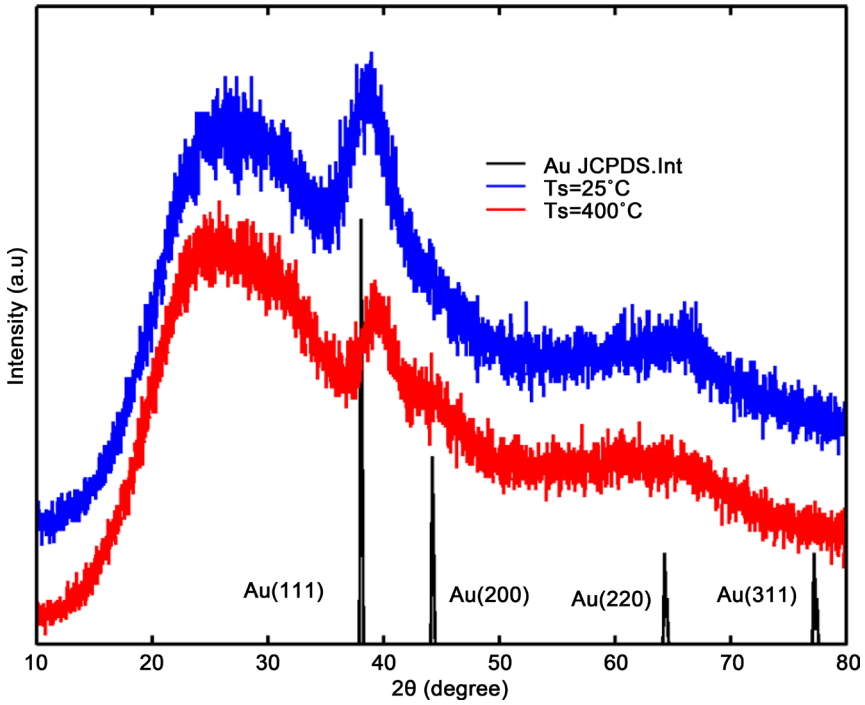

Figure 1. X-ray diffractograms of Au/SiO_2 nanocomposite thin films deposited at two substrate temperatures and JCPDS of gold thin film.

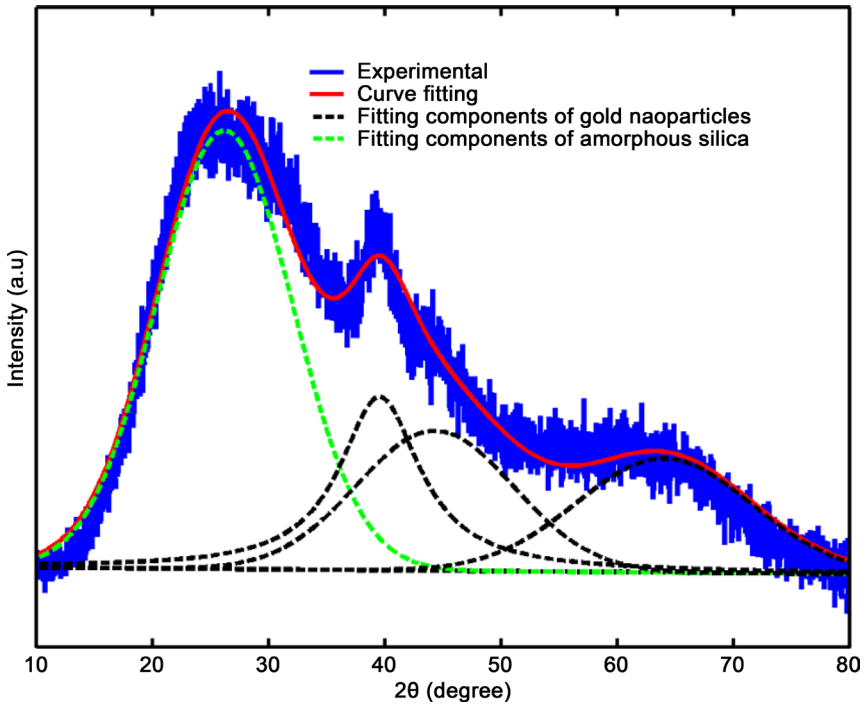

Figure 2. Experimental diffractogram of the sample deposited at T_S = 400˚C and their curve fitting where different pseudo-Voigt functions were taken into account.

peaks resulting from the fitting are attributed to the crystal planes of Au (111), Au (200) and Au (220). The peak positions are in agreement with the well-known data: JCPDS-04-04784 characteristic of the FCC cubic structure, indicating that

the small gold particles should adopt an fcc-like structure.

The crystallite sizes of AuNPs were calculated from the Debye-Scherer's formula using the FWHM in radians of the Au (111) reflection: $D = k\lambda/\beta \cdot \cos\theta_B$, where k is a constant (0.9), D is the crystallite size (in nm), λ is wavelength (0.15406 nm), β is full width at half maximum (FWHM in radian) and θ_B is the Bragg diffraction angle.

Table 2 summarizes the fitting parameters determined from the Au (111) orientation plane for all the samples. The results indicate that Au NPs size is increased with increasing the substrate temperature. The obtained sizes are 0.73 nm and 1.13 nm for the A_1 and A_2 series respectively.

In order to promote some structural and optical changes that will be required to tailor the SPR effect, the films were thermally annealed in air. The XRD spectra for two series A_1 and A_2 of Au/SiO_2 nanocomposite films as deposited and annealed at various temperatures are presented in Figure 3 and Figure 4.

For all the samples, characteristic peaks representing pure Au were not very prominent and no peak corresponding to SiO_2 was observed, indicating that after annealing process, there is no crystallized SiO_2 in these films. The X-ray spectra of the nanocomposite films have been deconvoluted in the same manner as previously mentioned. The results are reported in Table 2. The particle sizes, which were calculated from the Au (111) diffraction peak according to Scherrer's formula, varied from 0.73 nm to 1.08 nm for A_1 series and from 1.13nm to 1.54 nm for A_2 series, when heat temperature varies from 300˚C to 500˚C. With the increase of temperature, due to thermal expansion, the radius of the nanoparticle increases as:

$$R(T) = R_0\left(1+\beta\Delta T\right)^{1/3} \tag{1}$$

where R_0 is the nanoparticle radius at room temperature. At the increase of temperature, the volume of nanoparticle increases [31]:

$$V(T) = V_0\left(1+\beta\Delta T\right) \tag{2}$$

Table 2. Results of the curve fitting of the experimental diffractograms calculated from Au (111) reflections of the samples.

Samples Number	Temperature (˚C)	Bragg's angle 2θ (degree)	FWHM (degree)	Particle size (nm)
A_1	as deposited	39.76	11.64	0.73
	300˚C	39.19	9.40	0.89
	400˚C	39.38	8.63	0.97
	500˚C	39.39	7.77	1.08
A_2	as deposited	39.16	7.44	1.13
	300˚C	39.14	6.30	1.34
	400˚C	39.40	5.86	1.44
	500˚C	39.30	5.45	1.54

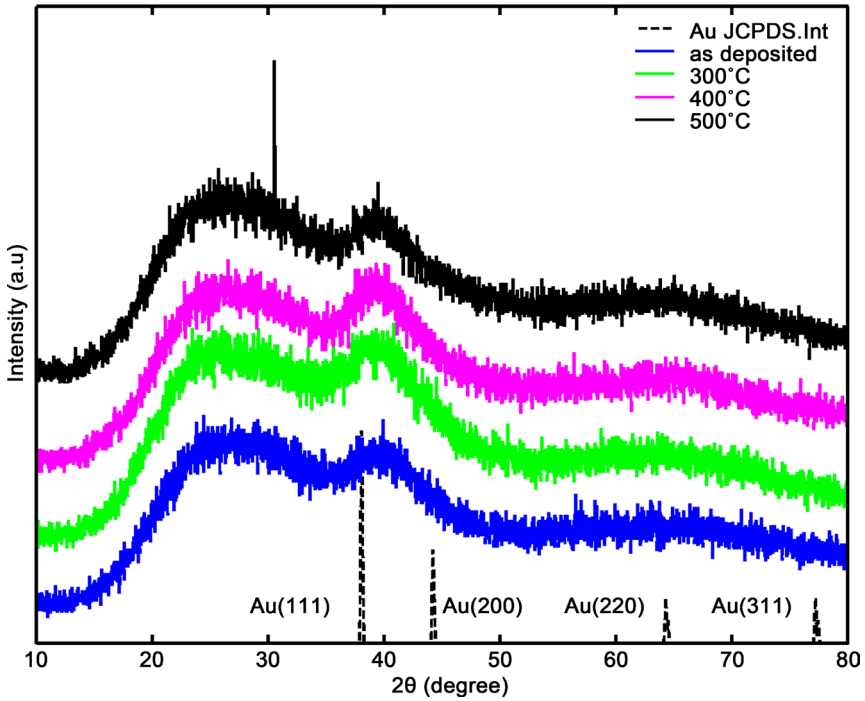

Figure 3. X-ray diffractograms of A_1 series, as-grown and heated at 300˚C, 400˚C, 500˚C and JCPDS of gold thin films.

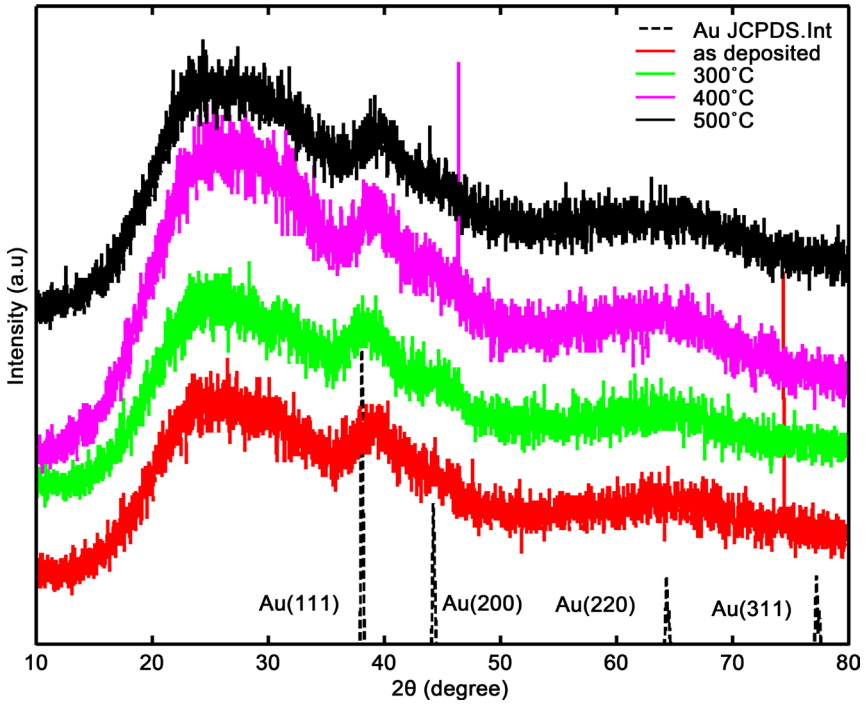

Figure 4. X-ray diffractograms of A_2 series, as-grown and heated at 300˚C, 400˚C, 500˚C and JCPDS of gold thin films.

where $\Delta T = T - T_0$ is the change of temperature from the room one and β is the volume expansion coefficient for gold nanoparticle. The graphical representation of the volume ratio V/V_0 of gold nanoparticle versus the annealing

temperature is shown in Figure 5 and Figure 6. So, from the slope of the linear regression, the volume expansion coefficient β for gold nanoparticle is evaluated according to the Equation (2).

The values of $\beta = 1.61\times10^{-5}/^{\circ}K$ and $\beta = 1.13\times10^{-5}/^{\circ}K$ have been obtained for the A_1 and A_2 series respectively. Note that we consider the thermal

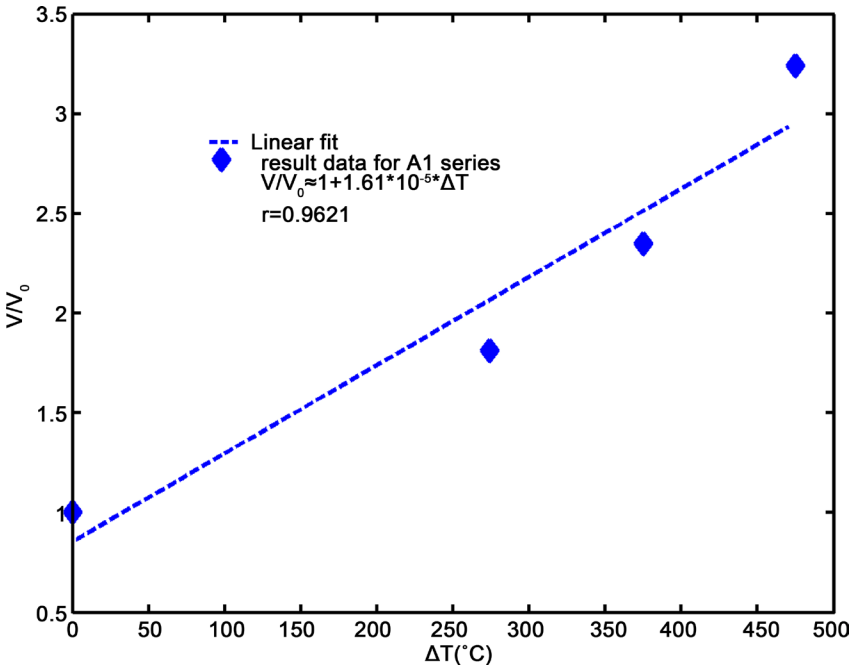

Figure 5. The plots of volume ratio of AuNPs calculated from Au (111) diffraction for A_1 series versus annealing temperatures.

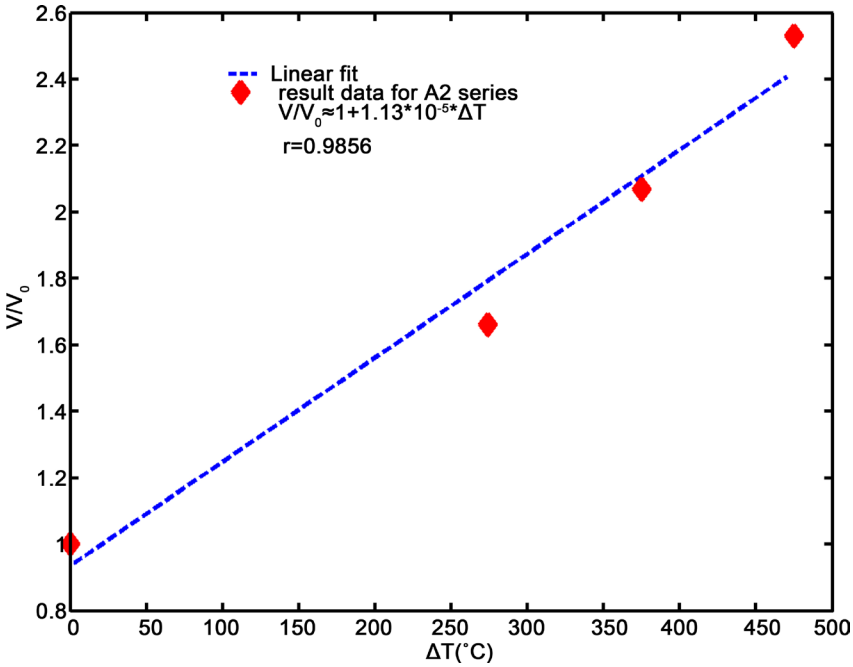

Figure 6. The plots of volume ratio of AuNPs calculated from Au (111) diffraction for A_2 series versus temperature.

expansion of a nanoparticle, by assuming that it is free. However, the nanoparticle is embedded in the silica matrix. Respectively, since the volume thermal expansion coefficient for silica is smaller ($1.65\times10^{-6}/^{\circ}K$ for fused silica) than one for gold $\left(4.17\times10^{-5}/^{\circ}K\right)$ [32], it seems at first glance that the silica host matrix would block the expansion of a nanoparticle. The obtained values are lower than the bulk. However, our procedure of annealing treatment of Au/SiO_2 composite samples occurs at the temperatures which are considerably higher than the temperature used in our measurements. After annealing, the samples were cooled down to room temperature. At cooling, both the nanoparticle and the hosting cavity contracted. But, due to a considerable difference of the coefficients of thermal expansion, the gold nanoparticle contracted considerably stronger, than the hosting cavity did. We can note that small-sized AuNPs have a slightly larger expansion coefficient than for larger particle sizes.

3.2. Optical Studies

Figure 7 shows the optical absorption spectra of Au/SiO_2 nanocomposite thin films deposited at two different substrate temperatures. It is observed in the case of the A_1 series, that for the as-deposited sample, no absorbance peak related the SPR peak characteristic of the gold particles could be observed. It indicates that the gold particle sizes are smaller than 2 nm [1]. On the other hand, in the case of A_2 series, the as-deposited sample shows an absorption band centered at 500 nm.

Figure 8 and Figure 9 show the absorbance spectra of Au/SiO_2 films as

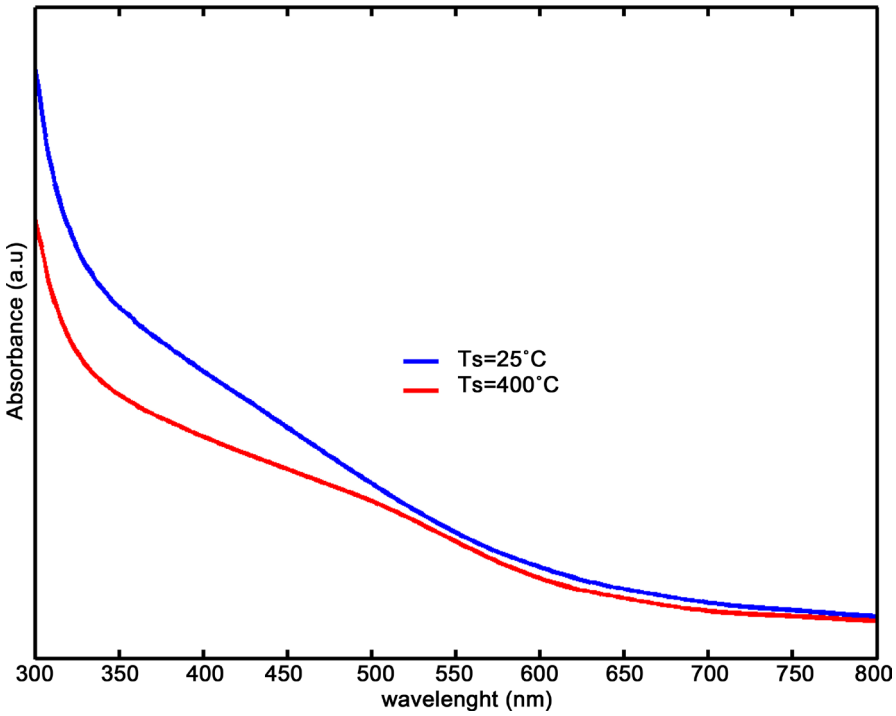

Figure 7. Optical absorption spectra of Au/SiO_2 nanocomposite films sputtered at two substrate temperatures.

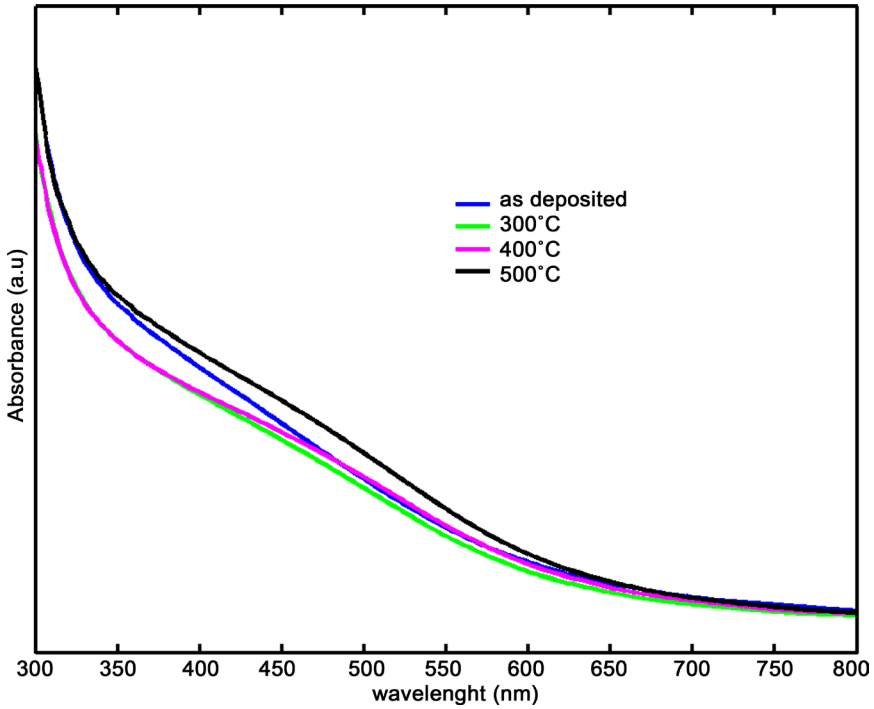

Figure 8. Optical absorption spectra of A_1 series as-deposited and at different annealing temperatures.

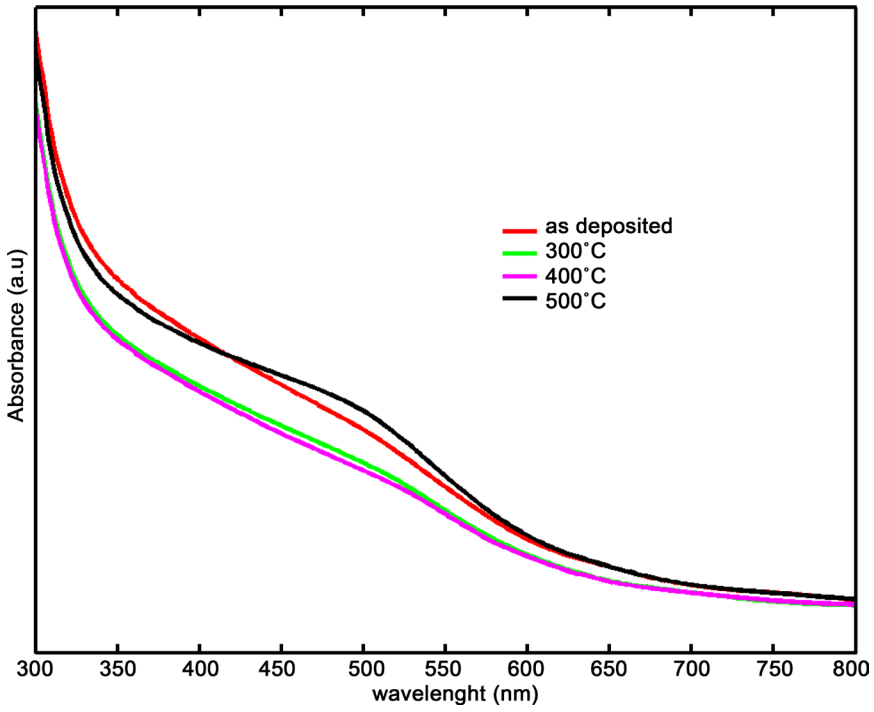

Figure 9. Optical absorption spectra of A_2 series as-deposited and at different annealing temperatures.

deposited and annealed at different temperature for the two series A_1 and A_2 respectively. It can be noted that after annealing, the films start to exhibit a broad and weak absorption band. Unlike in the A_1 series, broad band absorption is

observed for the as-deposited sample in A_2 series as seen in **Figure 9**. The intensity of the SPR absorption band decreases when the temperature varies from 25˚C to 400˚C and increases at 500˚C. It can be noted that the heating temperature has an appreciable effect on SPR band absorption when the annealing temperature is larger than that of the temperature deposition. So, from all the measured absorption spectra, it is not easy to determine the position of the SPR band and describe the trend of SPR bands in the samples.

In order to explain the absorption curves, a modelling of the spectra has been performed. Taking into account that particles are small compared to the wavelength of incident radiation the dipole approximation was applied. In this approximation, the absorption coefficient α for the medium with particles of volume V and number of particles per unit volume N is given by the following equation [33]:

$$\alpha(\lambda) = \frac{18\pi NV\varepsilon_m^{3/2}}{\lambda} \frac{\varepsilon_2}{\left(\varepsilon_1 + 2\varepsilon_m\right)^2 + \varepsilon_2^2} \tag{3}$$

where λ is the wavelength of the absorbing radiation, ε_m is the dielectric constant of the surrounding medium, ε_1 and ε_2 are the real and imaginary part of the dielectric function of particles. The dependence of the metal dielectric function on the size of the particles is taken into account using the model presented by Hövel *et al.* [34]:

$$\varepsilon(\lambda, D) = \varepsilon^{bulk}(\lambda) + \frac{\omega_P^2}{\omega^2 + i\omega\gamma_{bulk}} - \frac{\omega_P^2}{\omega^2 + i\omega\left(\gamma_{bulk} + 2A_{v_F}/D\right)} \tag{4}$$

where ε^{bulk} is the bulk gold dielectric constant, ω_P, v_F and γ_{bulk} being, the metal plasma frequency, the Fermi velocity and damping constant in the bulk respectively. A is a phenomenological parameter including details of the scattering process. The values of these parameters used in our simulation are those cited in the work [22] [23]. The dielectric constant values of the bulk were taken from [35]. Using the model described above by combining of Equations ((3), (4)) we fit the experimental optical spectra assuming a single uniform radius for all the clusters. The simulation and the experimental plots are shown in **Figure 10** and **Figure 11**. The parameter values deducted from this simulation are summarized in **Table 3**.

For A_1 series, the average size of Au particles in the samples A_1 is in the range of 2.01 - 2.04 nm obtained from the optical absorption spectra, the size effect on the SPR band shift can be ignored. For A_2 series, the plasmon peak positions just vary from 500 nm to 503 nm, and the size increases slightly from 2.01 nm to 2.3 nm when heating temperature increases from 25˚C to 500˚C. The changes occurring in the Au nanocrystals upon increasing temperature show, when the gold particle size exceed slightly the well-known critical size (≈2 nm), superimposed on the background, a broad surface plasmon band around 500 nm occurs characteristic of gold nanoclusters, due to surface plasmon resonance. Similar observations have been reported for other gold-dispersed dielectric materials:

Alvarez *et al.* [1] prepared passivated gold particles with sizes in the range 1.4 - 3.2 nm, found that with decreasing size, the SPR band broadened until it became unidentifiable for sizes less than 2 nm. Palpant *et al.* [36] found also, that the

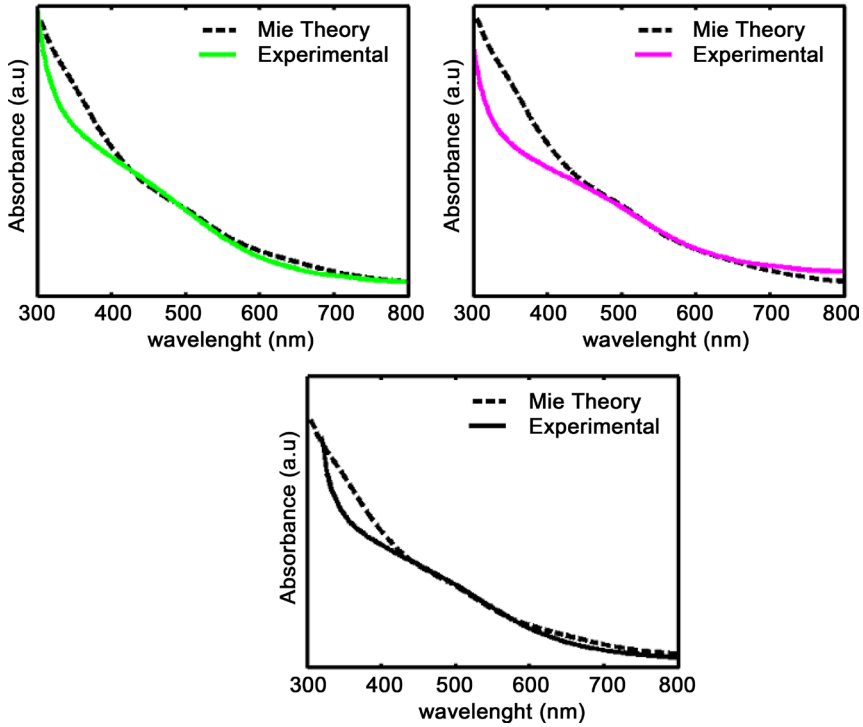

Figure 10. Experimental and Mie simulated optical absorption spectra for the A_1 series.

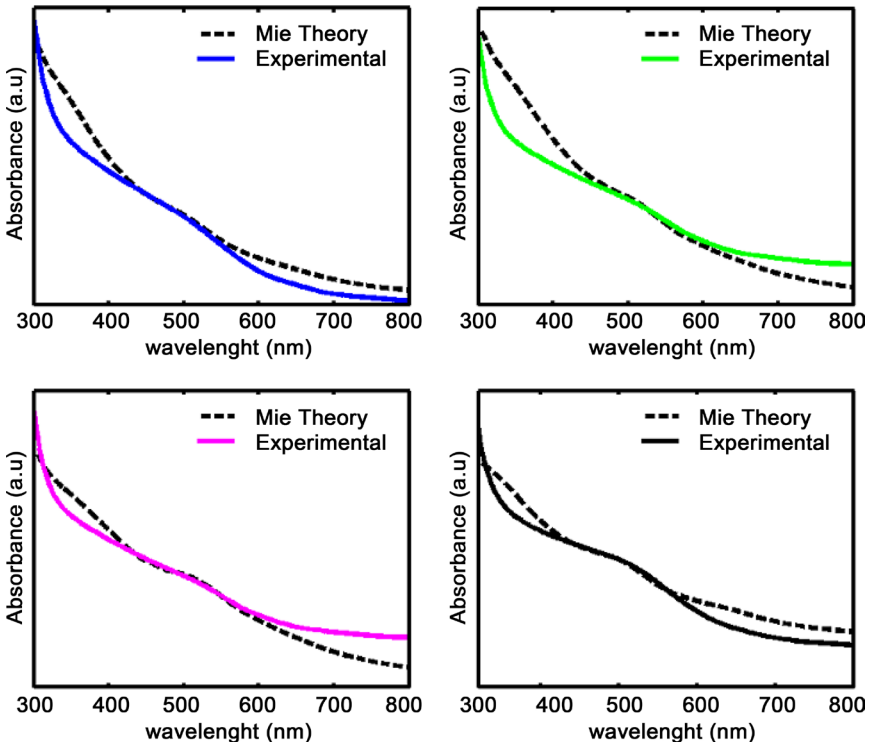

Figure 11. Experimental and Mie simulated optical absorption spectra for the A_2 series.

Table 3. Plasmon peak position, size and dielectric functions of the surrounding medium of the sample as-deposited and heating at different temperatures.

Samples Number	Temperature (˚C)	SPR(nm)	Particle size (nm)
A_1	as deposited	---	--
	300˚C	500	2.01
	400˚C	500	2.02
	500˚C	500	2.04
A_2	as deposited	500	2.01
	300˚C	501	2.1
	400˚C	501	2.1
	500˚C	503	2.3

plasmon absorption is damped and blueshifted with decreasing particle size, in the case of gold clusters in the size range 2 - 4 nm, embedded in alumina matrix grown by co-deposition technique using pulsed laser ablation.

4. Conclusions

The effect of substrate temperature (ambient and 400˚C) and thermal annealing on structural and optical properties of Au/SiO_2 nanocomposite films, prepared by RF-sputtering technique, have been investigated. The results of the present study lead to the following conclusions:

For the nanocomposite films grown at room temperature, formation of small gold nanoclusters with size below 2 nm inside the silica matrix was confirmed by XRD and optical absorption measurements. After annealing, the size of AuNPs is slightly larger than the critical size and the plasmon band peak position of gold clusters is around 500 nm.

As the substrate temperature increases to 400˚C, the SPR absorption band begins to appear at 500 nm wavelength indicating formation of gold nanoclusters. After annealing, the size of AuNPs increases slightly and the plasmon band peak position redshifts from 500 nm to 503 nm.

These experimental results show the ability to create and control very small gold clusters inside dielectric films, by a combination of the sputtering deposition parameters and subsequent heat-treatment.

Acknowledgements

We are grateful to Professor M.J.M. Gomes from the Centre of Physics, University of Minho, Portugal, for the experimental support.

References

[1] Alvarez, M.M., Khoury, J.T., Schaaff, T.G., Shafigullin, M.N., Vezmar, I. and Whetten, R.L. (1997) Optical Absorption Spectra of Nanocrystal Gold Molecules. *The Journal of Physical Chemistry B*, **101**, 3706-3712. https://doi.org/10.1021/jp962922n

[2] Link, S. and El-Sayed, M.A. (1999) Spectral Properties and Relaxation Dynamics of Surface Plasmon Electronic Oscillations in Gold and Silver Nanodots and Nanorods. *The Journal of Physical Chemistry B*, **103**, 8410-8426 https://doi.org/10.1021/jp9917648

[3] Moskovits, M. (1985) Surface-Enhanced Spectroscopy. *Reviews of Modern Physics*, **57**, 783-826. https://doi.org/10.1103/RevModPhys.57.783

[4] Metiu, H. and Das, P. (1984) The Electromagnetic Theory of Surface Enhanced Spectroscopy. *Annual Review of Physical Chemistry*, **35**, 507-536. https://doi.org/10.1146/annurev.pc.35.100184.002451

[5] Kelly, K.L., Coronado, E., Zhao, L.L. and Schatz, G.C. (2003) The Optical Properties of Metal Nanoparticles: The Influence of Size, Shape, and Dielectric Environment. *The Journal of Physical Chemistry B*, **107**, 668-677. https://doi.org/10.1021/jp026731y

[6] Kreibig, U. and Fragstein, C.V. (1969) The Limitation of Electron Mean Free Path in Small Silver Particles. *Zeitschrift für Physik*, **224**, 307-323. https://doi.org/10.1007/BF01393059

[7] Kreibig, U. and Genzel, L. (1985) Optical Absorption of Small Metallic Particles. *Surface Sciences*, **156**, 678-700. https://doi.org/10.1016/0039-6028(85)90239-0

[8] Noguez, C. (2007) Surface Plasmons on Metal Nanoparticles: The Influence of Shape and Physical Environment. *The Journal of Physical Chemistry C*, **111**, 3806-3819. https://doi.org/10.1021/jp066539m

[9] Kreibig, U. and Vollmer, M. (1995) Optical Properties of Metal Clusters. Springer, Berlin, Heidelberg. https://doi.org/10.1007/978-3-662-09109-8

[10] Doremus, R.H. (1964) Optical Properties of Small Gold Particles. *The Journal of Chemical Physics*, **40**, 2389-396. https://doi.org/10.1063/1.1725519

[11] Doremus, R.H. (1965) Optical Properties of Small Silver Particles. *The Journal of Chemical Physics*, **42**, 414-417. https://doi.org/10.1063/1.1695709

[12] Mulvaney, P. (2001) Metal Nanoparticles: Double Layers, Optical Properties, and Electrochemistry, in Nanoscale Materials in Chemistry. John Wiley & Sons, Inc., New York. https://doi.org/10.1002/0471220620.ch5

[13] Link, S. and El-Sayed, M.A. (1999) Size and Temperature Dependence of the Plasmon Absorption of Colloidal Gold Nanoparticles. *The Journal of Physical Chemistry B*, **103**, 4212-4217. https://doi.org/10.1021/jp984796o

[14] Takahiro, K., Oizumi, S., Morimoto, K., Kawatsura, K., Isshiki, T., Nishio, K., Nagata, S., Yamamoto, S., Narumi, K. and Naramoto, H. (2009) Application of X-Ray Photoelectron Spectroscopy to Characterization of Au Nanoparticles Formed by IonImplantation into SiO_2. *Applied Surface Science*, **256**, 1061-1064.

[15] Cesca, T., Maurizio, C., Kalinic, B., Scian, C., Trave, E., Battaglin, G., Mazzoldi, P. and Mattei, G. (2014) Luminescent Ultra-Small Gold Nanoparticles Obtained by Ion Implantation in Silica. *Nuclear Instruments and Methods in Physics Research Section B: Beam Interactions with Materials and Atoms*, **326**, 7-10.

[16] Ferrara, M.C., Mirenghi, L., Mevoli, A. and Tapfer, L. (2008) Synthesis and Characterization of Sol-Gel Silica Films Doped with Size-Selected Gold Nanoparticles. *Nanotechnology*, **19**, 65706-65714. https://doi.org/10.1088/0957-4484/19/36/365706

[17] Ruffino, F., Bongiorno, C., Giannazzo, F., Roccaforte, F., Raineri, V. and Grimaldi M.G. (2007) Effect of Surrounding Environment on Atomic Structure and Equilibrium Shape of Growing Nanocrystals: Gold in/on SiO_2. *Nanoscale Research Letters*, **2**, 240-247. https://doi.org/10.1007/s11671-007-9058-4

[18] Kerboua, C.H., Lamarre, J.M., Martinu, L. and Roorda, S. (2007) Deformation, Alignment and Anisotropic Optical Properties of Gold Nanoparticles Embedded inSilica. *Nuclear Instruments and Methods in Physics Research Section B: Beam Interactions with Materials and Atoms*, **257**, 42-46.

[19] Lamarre, J.M., Yu, Z., Harkati, C., Roorda, S. and Martinu, L. (2005) Optical and Microstructural Properties of Nanocomposite Au/SiO_2 Films Containing Particles Deformed by Heavy Ion Irradiation. *Thin Solid Films*, **479**, 232-237.

[20] Liao, H.B., Xiao, R.F., Fu, J.S., Yu, P., Wong, G.K. and Sheng, P. (1997) Large Third-Order Optical Nonlinearity in Au: SiO_2 Composite Films near the Percolation Threshold. *Applied Physics Letters*, **70**, 1-3. https://doi.org/10.1063/1.119291

[21] Tanahashi, I., Manabe, Y., Tohda, T., Sasaki, S. and Nakamura, A. (1996) Optical Nonlinearities of Au/SiO_2 Composite Thin Films Prepared by a Sputtering Method. *Journal of Applied Physics*, **79**, 1244-1249. https://doi.org/10.1063/1.361018

[22] Belahmar, A. and Chouiyakh, A. (2013) Effect of Post-Annealing on Structural and Optical Properties of Gold Nanoparticles Embedded in Silica Films Grown by RF Sputtering. *Advances in Physics Theories*, **15**, 38-46.

[23] Belahmar, A. and Chouiyakh, A. (2016) Investigation of Surface Plasmon Resonance and Optical Band Gap Energy in Gold/Silica Composite Films Prepared by RF-Sputtering. *Journal of Nanoscience and Technology*, **2**, 81-84.

[24] Belahmar, A. and Chouiyakh, A. (2017) Effect of Substrate Temperature on Structural and Optical Properties of Au/SiO_2 Nanocomposite Films Prepared by RF Magnetron Sputtering. *Open Access Library Journal*, **4**, e3810.

[25] Belahmar, A. and Chouiyakh, A. (2016) Structural and Optical Study of Au Nanoparticles Incorporated in Al2O3 and SiO_2 Thin Films Grown by RF-Sputtering. *International Journal of Advanced Research in Computer Science and Software Engineering*, **6**, 109-116.

[26] Yu, G.Q., Tay, B.K., Zhao, Z.W., Sun, X.W. and Fu, Y.Q. (2005) Ion Beam Co-Sputtering Deposition of Au/SiO_2 Nanocomposites. *Physica E: Low Dimensional Systems and Nanostructures*, **27**, 362-368.

[27] Zhuo, B., Li, Y., Teng, S. and Yang, A. (2010) Fabrication and Characterization Au/SiO_2 Nanocomposite Films. *Applied Surface Science*, **256**, 3305-3308.

[28] Belahmar, A. and Chouiyakh, A. (2016) Influence of Argon Pressure on the Optical Band Gap Energy and Urbach Tail of Sputtered Au/SiO_2 Nanocomposite Films. *International Journal of Advanced Research in Computer Science and Software Engineering*, **6**, 7-13.

[29] Sangpour, P., Akhavan, O., Moshfegh, A.Z. and Roozbehi, M. (2007) Formation of Gold Nanoparticles in Heat-Treated Reactive Co-Sputtered Au/SiO_2 Thin Films. *Applied Surface Science*, **254**, 286-290.

[30] Belahmar, A. and Chouiyakh, A. (2016) Sputtering Synthesis and Thermal Annealing Effect on Gold Nanoparticles in Al_2O_3 Matrix. *Journal of Nanoscience and Technology*, **2**, 100-103.

[31] Yeshchenko, O.A., Bondarchuk, I.S., Gurin, V.S., Dmitruk, I.M. and Kotko, A.V. (2013) Temperature Dependence of the Surface Plasmon Resonance in Gold Nanoparticles. *Surface Science*, **608**, 275-281.

[32] Kittel, C. (2005) Introduction to Solid State Physics. John Willey & Sons, New York.

[33] Mie, G. (1908) Contributions to the Optics of Turbid Media, Particularly of Colloidal Metal solutions. *Annalen der Physik*, **25**, 377-445. https://doi.org/10.1002/andp.19083300302

[34] Hovel, H., Fritz, S., Hilger, S., Kreibig, U. and Vollmer, U. (1993) Width of Cluster Plasmon Resonances: Bulk Dielectric Functions and Chemical Interface Damping. *Physical Review B*, **48**, 18178-18188. https://doi.org/10.1103/PhysRevB.48.18178

[35] Palik, E.D. (1991) Handbook of Optical Constants of Solids. Academic Press, New York.

[36] Palpant, B., *et al.* (1998) Optical Properties of Gold Clusters in the Size Range 2-4 nm. *Physical Review B*, **57**, 1963-1970. https://doi.org/10.1103/PhysRevB.57.1963